Research Article | Vol. 33, No. 13 / 30 Jun 2025 / Optics Express 28164
Optics EXPRESS

Buffer gas cooling of a continuous CO molecular beam

AMAN GANGWAR,[1] TOMMASO VEDOVELLO,[2] FRANCESCO PIO MERAFINA,[3] GIACOMO INSERO,[1,4,5] SIMONE BORRI,[1,4] PAOLO DE NATALE,[1,4] GABRIELE SANTAMBROGIO,[1,4,6,*] AND SAGAR SUTRADHAR[1,4]

[1]*European Laboratory for Nonlinear Spectroscopy, LENS, Via Nello Carrara 1, 50014 Sesto Fiorentino, Italy*
[2]*Dipartimento di Fisica e Astronomia, University of Florence, Via Sansone 1, 50014 Sesto Fiorentino, Italy*
[3]*Università di Bari, Piazza Umberto I, 1, 70121 Bari, Italy*
[4]*Istituto Nazionale di Ottica, CNR, Largo E. Fermi 6, 50125 Firenze, Italy*
[5]*Department of Experimental and Clinical Biomedical Sciences "Mario Serio", University of Florence, Viale G. Pieraccini 6, 50139 Florence, Italy*
[6]*Istituto Nazionale di Ricerca Metrologica, INRIM, Via Nello Carrara 1, 50019 Sesto Fiorentino, Italy*
[*]*santambrogio@lens.unifi.it*

Abstract: We characterize a continuous buffer gas cooled source using CO molecules. We show results about the source performance considering different parameters, like gas flow rate, nozzle size, and internal cell volume. The beam contains 2.5×10^{14} molecules/(s sr) at about 160 m/s. Moreover, for two rotational states we observe an unexpected population distribution that we tentatively attribute to a lower temperature inside the cell. Considering the importance of buffer-gas cooling for experiments on ultracold molecules prepared with direct laser cooling, we believe that our work will improve this key first-stage cooling, accelerating the adoption of molecules in the framework of quantum technologies.

© 2025 Optica Publishing Group under the terms of the Optica Open Access Publishing Agreement

1. Introduction

Ultracold molecules are very promising candidates for advancing modern physics, with applications ranging from fundamental physics to frontier technologies such as quantum simulation and quantum computation [1,2]. This is due to their rich internal structure, symmetry, and strong intramolecular fields, which make them ideal systems for investigating new physics. However, this same complexity poses significant challenges for cooling and detection, making these processes much more difficult compared to atoms. To overcome these difficulties, a first cooling stage is usually applied to the molecular sample. Virtually all current experiments with laser-cooled molecules rely on a buffer gas source [3,4]. In this source, molecules are injected or produced inside the cell, where they thermalize with a cold rare buffer gas, typically helium or neon. The molecular beam exiting the source is usually in an intermediate regime between effusive and hydrodynamic, i.e., experiencing almost no or a few collisions, respectively, at the exit aperture.

Buffer gas cooling techniques have been successfully applied to a variety of species, spanning a broad spectrum of chemical properties, including alkali atoms [5,6], alkaline earths [7], metals [8], chemically reactive polar molecules [9–11], and polyatomic molecules [12].

In this work, we present our newly-developed buffer gas source that we characterize using carbon monoxide. Although CO is not a particularly interesting species for laser cooling, it has the advantage of being easily available in a bottle. Moreover, by exciting CO to its first excited, metastable, electronic state, the $a^3\Pi$ state, characterisation of the beam is straightforward. With the present setup for a continuously seeded buffer gas beam, we can calculate the overall efficiency of the source from the know amount of gas that we let into the system and the number

#560951 https://doi.org/10.1364/OE.560951
Journal © 2025 Received 5 Mar 2025; revised 3 Jun 2025; accepted 3 Jun 2025; published 25 Jun 2025

Optics EXPRESS

of cold molecules in the beam. Such measurements are extremely hard when the species of interest are produced via laser ablation and/or chemical reaction. Intense effusive beams can be produced with other molecules, too, [7] but CO is particularly advantageous given its relatively low freezing temperature.

We optimized the source for maximal flux and minimal velocity of the molecular beam trying various combinations of nozzle sizes and cell lengths. We also measure molecules in two different rotational states in order to estimate rotational thermalization inside the cell and provide an estimation of the beam temperature.

2. Theoretical description of the dynamics within a buffer gas cell

Buffer-gas cooling of atoms or molecules relies on collisions with cold buffer gas atoms at cryogenic temperatures, bringing the target species to low temperatures. The buffer gas dissipates the translational and internal energy of the target species, ideally without chemical reaction or cluster formation. This method of energy dissipation is independent of any specific energy level structure, making it applicable to a wide range of target species [7].

A comprehensive overview of the dynamics in a buffer gas cell can be found in Refs. [4,9]. Here, we focus on outlining the key parameters associated with our setup.

Consider a buffer gas cell with a volume defined by $V_{\text{cell}} = A_{\text{cell}} \times L_c$, where L_c is the length of the cell interior and A_{cell} is the cross-sectional area. Typically, L_c is of the order of a few centimeters, and A_{cell} of a few cm^2. The cell is maintained at a fixed temperature T by a cryogenic refrigerator, typically between 1 K and 20 K. We use helium as buffer gas.

2.1. Buffer gas flow through the cell

The buffer gas exits the cell through a round aperture with diameter d_{aperture} of a few millimeters. The flow rate of the buffer gas, He in our case, is typically measured in standard cubic centimeters per minute (SCCM), where 1 SCCM is approximately equivalent to a flow of 4.5×10^{17} gas particles per second. Under steady-state conditions, the number density of helium atoms in the buffer cell, n_{He}, can be estimated by considering the constant flow of helium into the cell, f_{He}, and the pumping speed through the aperture [4],

$$n_{\text{He}} = \frac{4 f_{\text{He}}}{A_{\text{aperture}} \bar{v}_{\text{He}}}, \tag{1}$$

where $\bar{v}_{\text{He}}$ is the mean thermal velocity of the helium atoms near the aperture. For a typical flow of 1 SCCM of helium through an aperture with a diameter of 3 mm in a buffer cell maintained at a temperature of around 4 K, the number density is $n_{\text{He}} \approx 2 \times 10^{15}\,\text{cm}^{-3}$. The properties of the target species emerging from the buffer cell are solely determined by collisions with the buffer gas, which can be quantified by the mean free path. The mean free path is defined as $\lambda_{\text{CO}} = 1/(n_{\text{He}} \sigma_{\text{CO-He}} \sqrt{m_{\text{CO}}/m_{\text{He}} + 1})$, where σ is a collisional cross section and m a mass. To a good approximation [9], $\sigma_{\text{CO-He}} \approx \sigma_{\text{He-He}}$ and $\sigma_{\text{He-He}} \sim 10^{-14}\,cm^2$ [13].

The Reynolds number (Re) is an important figure of merit for the description of a gas flow. For the buffer gas flows through an aperture of diameter d_{aperture}, the Reynolds number can be approximated as,

$$\text{Re} \approx \frac{2\, d_{\text{aperture}}}{\lambda_{\text{He}}}, \tag{2}$$

where λ_{He} is the mean free path for the collisions of buffer gas atoms and it is expressed as, $\lambda_{\text{He}} = 1/(\sqrt{2}\, n_{\text{He}}\, \sigma_{\text{He-He}})$. Therefore, the Reynolds number can be expressed as,

$$\text{Re} \approx \frac{8\sqrt{2} f_{\text{He}}\, \sigma_{\text{He-He}}}{\pi d_{\text{aperture}} \bar{v}_{\text{He}}}. \tag{3}$$

Optics EXPRESS

The flow regimes can be categorized into three distinct types based on the Reynolds number, which reflects the extent of collisional interactions near the cell aperture. In the effusive regime ($\mathrm{Re} \lesssim 1$), few or no collisions occur near the aperture, and the beam properties align with the thermal distribution inside the cell. Moving into the intermediate or partially-hydrodynamic regime ($1 \lesssim \mathrm{Re} \lesssim 100$), collisions begin to influence the beam properties, although the flow does not yet exhibit fully fluid-like characteristics. Finally, in the hydrodynamic regime ($\mathrm{Re} \gtrsim 100$), the buffer gas behaves like a fluid, and the beam properties start to resemble those of a supersonic expansion, leading to a colder and less divergent beam.

2.2. Extraction efficiency of the cell

The particles of the target species can be depleted from the cooling region of the buffer cell through two primary processes: diffusion and entrainment. In the diffusion process, a significant fraction of particles may collide with, and adhere to, the walls of the cell, while only a very small fraction diffuse out through the aperture. The effectiveness of diffusion through the aperture is governed by the ratio of the aperture area to the surface area of the cooling region, which is typically $\leq 1\%$. Consequently, for the remainder of this discussion, we assume that the diffusion process predominantly results in particle losses, thereby limiting the extraction efficiency of particles from the buffer gas cell. In contrast, the second process involves entrainment, where particles are extracted or "pumped out" by the helium flow continuously emerging through the aperture.

Considering the diffusion and the entrainment processes, we define two characteristic time scales for particle movement within the cell. The diffusion time scale, τ_{diff}, represents the time required for particles of the target species to diffuse to the walls of the cooling region. The pump-out time scale, τ_{pump}, represents the time it takes for these particles to traverse the cell under the influence of helium flow. Following Ref. [4], we can write

$$\tau_{\mathrm{diff}} = \frac{16\, A_{\mathrm{cell}}\, n_{\mathrm{He}}\, \sigma_{\mathrm{CO\text{-}He}}}{9\,\pi\,\bar{v}_{\mathrm{He}}} \tag{4}$$

and

$$\tau_{\mathrm{pump}} = \frac{4\, V_{\mathrm{cell}}}{\bar{v}_{\mathrm{He}} A_{\mathrm{aperture}}} \tag{5}$$

The diffusion and pump-out times are typically around 1–10 ms. The efficiency of particle extraction from the cell is governed by the interplay between these two time scales. Therefore, it is instructive to define a dimensionless parameter

$$\gamma_{\mathrm{cell}} \equiv \frac{\tau_{\mathrm{diff}}}{\tau_{\mathrm{pump}}} = \frac{4}{9\pi} \frac{n_{\mathrm{He}} \sigma_{\mathrm{CO\text{-}He}} A_{\mathrm{aperture}}}{L_{\mathrm{cell}}} \approx \frac{\sigma_{\mathrm{CO\text{-}He}} f_{\mathrm{He}}}{L_{\mathrm{cell}} \bar{v}_{\mathrm{He}}}. \tag{6}$$

The value of γ_{cell} defines the regime of particle extraction. For instance, $\gamma_{\mathrm{cell}} \lesssim 1$ corresponds to the "diffusion limit", where particles diffuse to the wall faster than they are extracted from the cell. This regime results in a low output flux of target particles. In contrast, when $\gamma_{\mathrm{cell}} > 1$, the system operates in the "hydrodynamic regime", resulting in a beam rich in target species.

While γ_{cell} can estimate the extraction efficiency well, there are instances where this simple estimate breaks down. For example, γ_{cell} has no explicit dependence on the aperture diameter; however, it has been observed experimentally that decreasing the cell aperture diameter can reduce the extraction efficiency. [14,4] These measurements suggest that the cell aperture diameter should not be too small (less than 3 mm) to achieve good extraction. It is thus helpful to determine empirically the optimal cell geometry. The gas flow regime, described by the Reynolds number, Eq. (3), and the extraction parameter γ_{cell}, Eq. (6) are related by a factor that depends on

Optics EXPRESS

geometry:

$$\frac{\gamma_{\text{cell}}}{\text{Re}} \propto \frac{d_{\text{aperture}}}{L_{\text{cell}}}. \tag{7}$$

This means that, at least in principle, it is possible to separately control the extraction efficiency (governed by γ_{cell}) and the flow regime (governed by Re). Most buffer gas sources operate in either the effusive or the intermediate flow regimes, and it is experimentally challenging to design a beam that is completely effusive, has good extraction, and has sufficient thermalization.

2.3. Thermalization of CO molecules

As previously mentioned, the characteristics of the target particles emerging from the buffer cell are determined by the collisions with buffer gas atoms. The translational temperature of the CO molecules, T_{CO}, after undergoing N collisions with the buffer gas, can be estimated as follows [4],

$$\frac{T_{\text{CO}}(N)}{T_{\text{He}}} \approx 1 + \frac{T_{\text{CO}}(0)}{T_{\text{He}}} e^{-N/\kappa}, \tag{8}$$

where $\kappa = (m_{\text{CO}} + m_{\text{He}})^2/(2\, m_{\text{CO}}\, m_{\text{He}})$, T_{He} is the temperature of the buffer gas atoms in the cell, $\sim$ 4 K, and $T_{\text{CO}}(0)$ is the temperature of the target particles when they are introduced into the cell, $\sim$ 70 K (see below). Using this formula, we estimate that for CO molecules in the buffer cell, about 30 collisions are needed to translationally cool the molecules from room temperature to within 2.5% of the temperature of the buffer gas atoms. For typical values of $\sigma_{\text{CO-He}} \approx 10^{-14}\,\text{cm}^2$ and He number density of $10^{15-16}/\text{cm}^3$, the mean free path is $0.01 - 0.2$ mm. Therefore, the thermalization length for the species in the buffer gas cell is typically no more than $30 \times 0.2\,\text{mm} = 6\,\text{mm}$.

Apart from translational cooling of the target species, buffer gas cooling is also effective at rotational quenching which is driven by the anisotropy of the helium interaction with the molecule [15]. Typical rotational relaxation cross sections for molecules with helium buffer gas are of the order $\sigma_{\text{rot}} \sim 10^{-(15-16)}\,\text{cm}^2$ [16], which means that around $\sigma_{\text{CO-He}}/\sigma_{\text{rot}} \sim 10 - 100$ collisions are required to relax a rotational state. With the parameters given above, we estimate that a cell length of 9–90 mm is required for full rotational quenching.

2.4. Forward velocity of the CO beam

In the intermediate regime, the average velocity of the Helium, $\bar{v}_{\text{He}}$, is higher than that of CO, $\bar{v}_{\text{CO}}$, by a factor of $\sqrt{m_{\text{CO}}/m_{\text{He}}}$. The collisions of the Helium atoms with the CO near the aperture are predominantly in the forward direction. Therefore, the CO molecules are accelerated in the forward direction, which results in a velocity larger than the thermal velocity of the CO molecules in the cell.

CO molecules undergo approximately $\frac{\text{Re}}{2}$ collisions near the aperture [14]. For a small number of collisions, the resulting forward velocity is given by [4],

$$v_{\text{CO}} \approx \bar{v}_{\text{CO}} + 0.6\, \bar{v}_{\text{He}}\, \text{Re}\, \frac{m_{\text{He}}}{m_{\text{CO}}} \tag{9}$$

This suggests a linear increase of forward velocity with Re ($1 \lesssim \text{Re} \lesssim 10$) and therefore with buffer gas flow. However, as v_{CO} approaches $\bar{v}_{\text{He}}$, the above model breaks down, as the maximum possible forward velocity of the CO molecules is $1.4\bar{v}_{\text{He}}$ as determined by the fully hydrodynamic expansions of the helium atoms [4]. We therefore expect that the forward velocity should saturate to this value at large enough *Re*. For $\text{Re} \gtrsim 10$, the forward velocity is described by the "sudden freeze" model,

$$v_{\text{CO}}(\text{Re}) \approx 1.4\bar{v}_{\text{He}} \left(1 - \frac{4}{\text{Re}^{4/5}}\right) \tag{10}$$

The transition to sudden-freeze model occurs at the flow rate for which there are collisions at a distance larger than one aperture diameter from the aperture. This happens for $\text{Re} \gtrsim 10$ [14].

Optics EXPRESS

For sufficiently high Re (specifically Re $\gtrsim$ 100), species can achieve a forward velocity of

$$v_{\mathrm{CO}} \approx 1.4\bar{v}_{\mathrm{He}} \tag{11}$$

3. Experimental system

A schematic of the vacuum system is shown in Fig. 1. The vacuum system consists of two chambers. The first chamber contains the buffer gas cell, which is connected to a two-stage pulse tube cryostat (PT425, Cryomech). The second chamber houses the detection region. Both chambers are pumped by turbo-molecular pumps, HiPace 1200 and HiPace 300 (Pfeiffer Vacuum), for the first and second chamber, respectively. The system typically operates at a pressure of approximately $\sim 10^{-7}$ mbar, which limits the number of collisions with background gas, thereby facilitating the formation of a molecular beam. The pressure is measured in both chambers at the room-temperature part of the chambers.

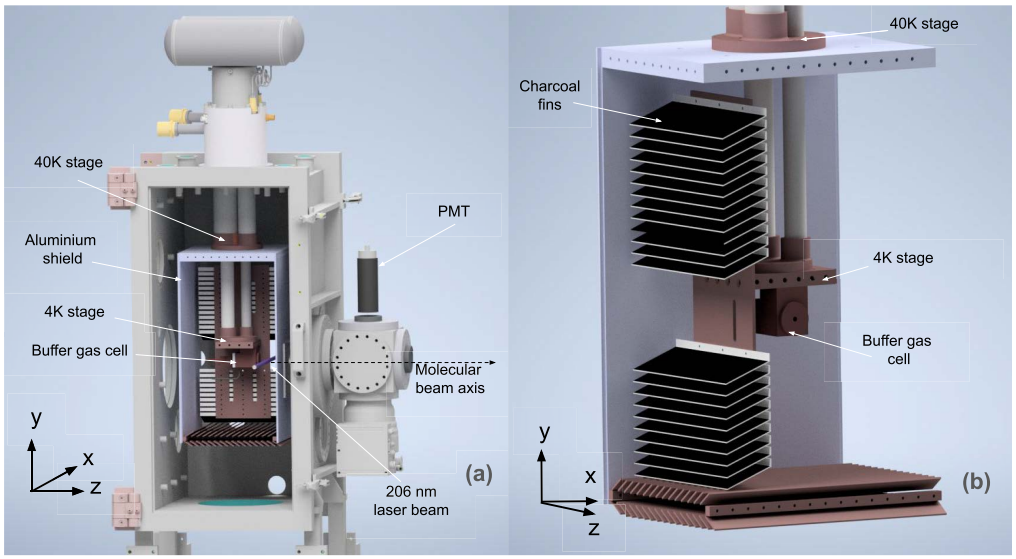

Fig. 1. Overview of the overall vacuum system (a) and a detailed arrangement of the buffer cell (b). Charcoal grains are glued to copper fins (as described in the text) and attached to a 4K cold head. For the visual clarity, only one of the charcoal fin arrangement is shown, on two different sides in the two pictures to avoid obstructing the view of the cell. The bottom of the radiation shield is closed by a series of copper stripes arranged in a chevron shape.

An aluminum shield is mounted in contact with the 40-K stage of the cryostat, while the buffer cell is attached to the 4-K stage. The aluminum shield functions as a radiation shield, effectively reducing the thermal radiation load on the buffer cell. A ~23 mm hole at the front of the radiation shield serves as an aperture for the molecular beam to emerge. Additionally, two orthogonal ports on the radiation shield, positioned perpendicular to the molecular beam, provide access for the excitation laser. The excitation laser intercepts the molecular beam approximately 30 mm after the cell nozzle. To further minimize the thermal load on the buffer cell, the radiation shield is wrapped 10 layers of polyester foil, double-sided aluminized, perforated and interleaved with 10 layers of non-woven polyester spacer material.

Charcoal at cryogenic temperatures is well known for its ability to efficiently absorb helium. [17] In many cryogenic buffer gas beam sources, the cell is surrounded by a small metal enclosure maintained at 4K, with charcoal glued on its interior walls. Instead, we developed a skeletal like copper structure mounted to the 4K head of the cryostat. Fine charcoal grains are glued

Optics EXPRESS

to the copper fins using a thin layer of thermally conductive epoxy glue. These fins are then integrated into the copper framework, which is connected to the 4K cold head. This solution substantially increases the area covered by charcoal, thereby enhancing helium pumping capacity, while maintaining good conductance toward the turbo pump. The large copper surface covered by charcoals allows for continuous pumping of 20 SCCM of Helium for over 2 days without using the turbo pump before heating the system to release the adsorbed helium, a value much higher compared to other systems.

3.1. Design of the buffer gas cell

The schematic of the buffer gas cell is shown in Fig. 2. The top part of the cell is attached to the 4K cold head of the cryostat. The cell is machined from a copper block and features a cylindrical region, which we refer to as the "cooling region". The temperature measured at the cell under normal operation conditions is of 3.7 K.

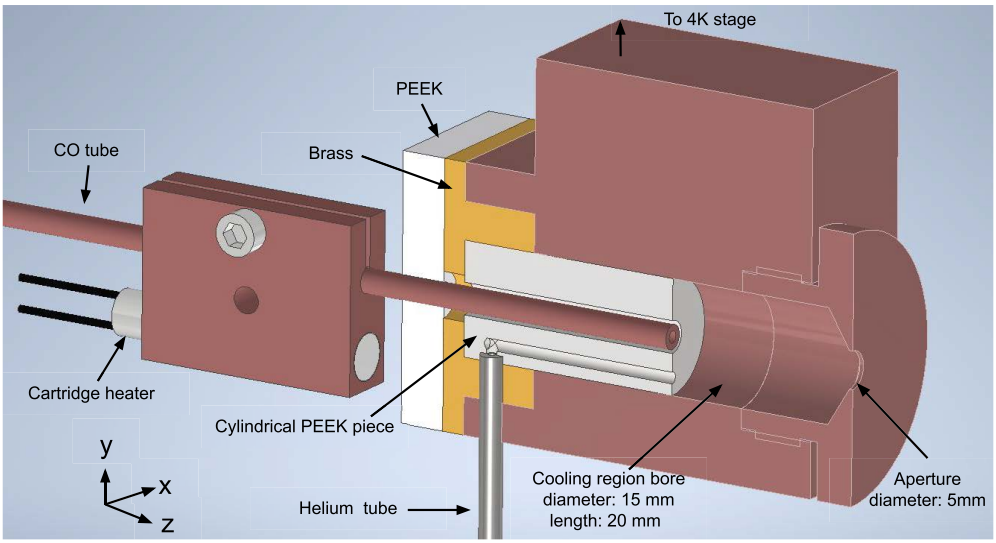

Fig. 2. The cross-sectional view of the buffer cell illustrates the arrangement of the aperture and the gas inlet tubes for CO and helium. A polyether ether ketone (PEEK) component is employed to thermally isolate the CO inlet tube from the cold buffer cell, as described in the text. Furthermore, a cylindrical PEEK piece is integrated to precisely control the length of the cooling region. The temperature of the CO tube near the buffer cell is regulated using a cartridge heater mounted on a copper element.

The nozzle of the cell is machined from a separate copper piece and subsequently attached to the buffer cell with a specific threading, facilitating a systematic study of how aperture dimensions determine the system performance. The cooling region is designed as a cylinder with a diameter of 15 mm. The exit nozzle has a conical shape, as outlined in [18]. The gas inlet configuration for the buffer cell is depicted in Fig. 2. To precisely control the cooling region length, cylindrical PEEK pieces are attached to the back end of the cell. These PEEK pieces feature appropriately sized holes to allow helium flow into the cooling region, as shown in Fig. 2. By incorporating these pieces, we reduced the overall length of the cell, allowing for controlled variation of the cooling region length. In this study, we tested nozzles with diameters of 2, 3, 4, and 5 mm, and cooling region lengths of 2, 3, 4, and 5 cm.

Helium and CO gases are supplied to the buffer gas cell from their respective bottles, with the flow rates of both gases controlled by flowmeters (MCE-20SCCM-D-6MMCOMP for helium

Optics EXPRESS

and MCE-1SCCM-D-6MMCOMP for CO, by Alicat). The helium line passes through a cooling cell soldered to the 4-K stage of the cryostat. The cold helium is injected into the buffer cell via a stainless steel capillary tube with an outer diameter of 3.2 mm, as depicted in Fig. 2. The CO gas is introduced from the back end of the cell through a 3.2-mm-outer-diameter copper capillary tube. This tube is thermally isolated from the buffer cell by a PEEK piece, and cartridge heaters are used to keep the CO line at 70 K by a PID controller to prevent freezing. This heating arrangement is illustrated in Fig. 2. Under standard pressure, CO liquefy at 81.15 K and freezes at 74.15 K.

3.2. Optical transitions, detection, and the laser system

To detect CO molecules emerging from the buffer cell, we first excite them to a metastable triplet state with a pulsed laser. 1 mJ of light at 206 nm saturates the spin-forbidden transition $a^3\Pi_1(v=0, J=1) \leftarrow X^1\Sigma^+(v=0)$. The $a^3\Pi_1(v=0, J=1)$ has a lifetime of 2.63 ms. [19] Then, we detect their phosphorescence on a photo-multiplier tube (PMT) (9813BQ, ET Enterprises), positioned approximately 24.5 cm downstream from the excitation region. It has an efficiency of 30% at 206 nm and it is mounted behind a quartz window with a transmission of 90% at 206 nm. The PMT is 117 mm from the axis of the molecular beam and has an effective entrance aperture of 35 mm in diameter. Such geometry allows for the collection of phosphorescence signal under 0.07 sr. All together these parameters yield a total detection efficiency of 0.135%. We show a scheme of this setup in Fig. 3. We acquire the phosphorescence signal with 13 μs resolution. For the range of velocities studied in this work (100–250 m/s), this set of parameters yields a velocity resolution of about ±10 m/s and detection efficiency is independent on velocity in first approximation. A first aperture in the 40-K shield reduce the divergence of the beam, but the field of view of the PMT further reduce the portion of the beam that is detected, yielding an overall divergence of 0.012 sr. This value is large but we believe that it is a useful measure because with high-power lasers one can decelerate and transverse-cool beams with such characteristics.

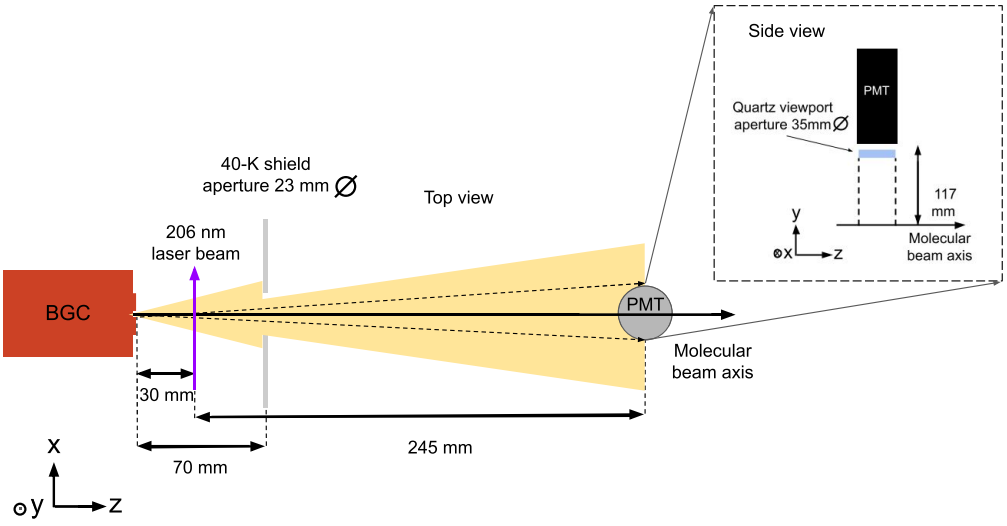

Fig. 3. Scheme of the molecular beam and detection system.

The electronic ground state $X^1\Sigma^+$ is best described in Hund's case (b), where the rotational states are fully characterized by the rotational quantum number N. The parity of the rotational states follows $(-1)^N$. In contrast, the rotational structure of the electronically excited state $a^3\Pi_1$ is described by the total angular momentum quantum number J. We characterized the buffer gas

Optics EXPRESS

cell by exciting the CO molecules from the rotational levels $N = 0$ to the lower component of the Λ doublet in the $a^3\Pi_1$ ($J = 1$) state. Only for the data shown in Fig. 8, we excite molecules also from the $N = 1$ level to the upper component of the Λ doublet in the $a^3\Pi_1$ ($J = 1$) state. A more detailed description of the energy levels can be found in Ref. [20].

We employed a laser system similar to that described in Ref. [21], which generates a pulsed beam with an energy of approximately 1 mJ at 206 nm, a repetition rate of 10 Hz, a pulse duration of around 6 ns and a linewidth of approximately 200 MHz.

4. Results and discussions

Figure 4 shows the phosphorescence signal detected by the PMT, both in the presence and absence of helium flow in the cell. We correct for the exponential decay of the population in the excited states and take the overall detection efficiency into account to calculate the number of molecules/(s sr) that have been prepared by the laser in a single quantum state.

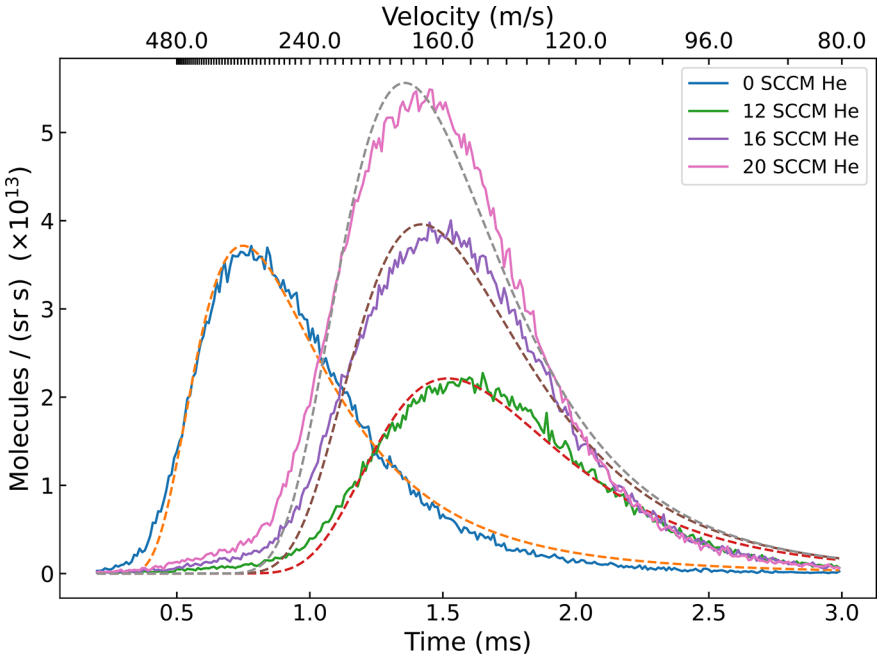

Fig. 4. Arrival time of CO molecules in front of the PMT with 1 SCCM of CO, and 0 and 12, 16, 20 SCCM of helium, a 3-cm cell length and 5-mm aperture, solid lines. The dashed lines are the fit of a Maxwell-Boltzmann distribution to the data. On top, the arrival time is converted into the correspondent molecular velocity.

Knowing the CO excitation time and the phosphorescence time, and the distance between excitation laser and PMT, we calculate the velocity of the molecular beam, shown on the horizontal axis on top of the graph. The shift in the overall profile and in the forward velocity in dependence of the helium flow clearly indicate the cooling effect on CO. We attribute this effect to the thermalization of CO molecules within the buffer cell. Collisions with He atoms might transfer part of the metastable population to the lower rotational states of the $\Omega = 0$ manifold on the $a^3\Pi$ state. However, the lifetime of those states are about two orders of magnitude longer than from the $\Omega = 1$ states. Therefore, we consider their contribution to the observed signal to be negligible.

Optics EXPRESS

Fitting the time of flight profiles in Fig. 4 to a Maxwell-Boltzmann distribution yields temperatures of 69.2 ± 0.1 K and 6.9 ± 0.2 K for helium flow rates of 0 and 20 SCCM, respectively. Two different effects are responsible for the observed data. Collisions with helium lower the CO velocity from the over 250 m/s expected for CO at around 70 K (temperature of the CO line) to below 150 m/s. However, by further increasing the He flow, we increase the Reynolds number and slightly accelerate CO molecules.

Figure 5 shows the CO phosphorescence signal in dependence on the He flow rate, for all source configurations. We see a monotonic signal increase with increasing flow, up to 20 SCCM, which is the limit of our He flowmeter. The same is true for the CO flow rate, which is limited to 1 SCCM by the CO flowmeter. Therefore, all data shown in the following are measured with 1 SCCM of CO and 20 SCCM of He.

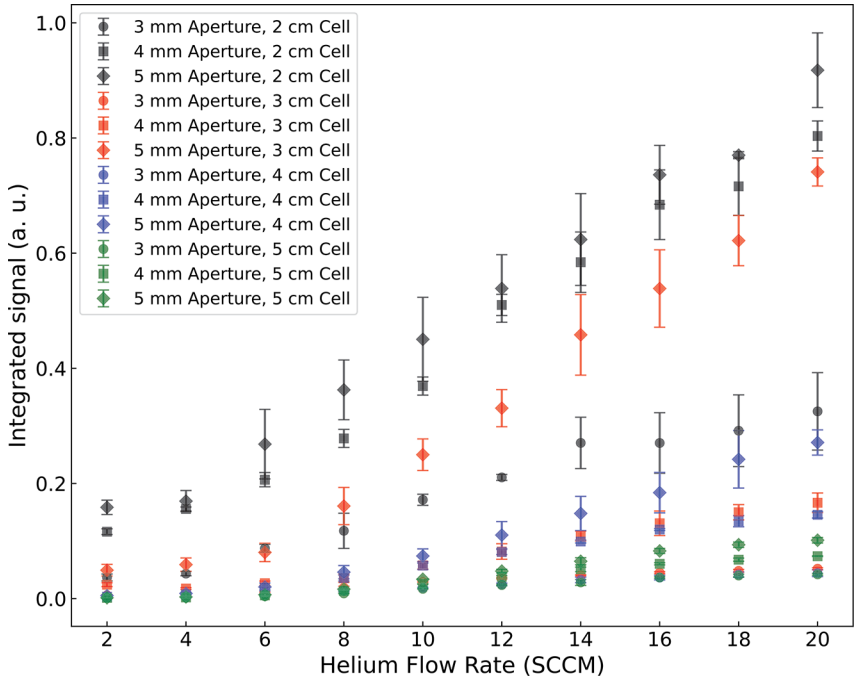

Fig. 5. Integrated phosphorescence signal in dependence on He flow rate, for all aperture diameters and cell lengths. In all cases, larger He flow yields larger CO signal.

We test Eq. (6) by measuring the phosphorescence signal in dependence on the cell length for various nozzle sizes, Fig. 6. A shorter cell minimizes the probability of diffusion to the walls and thus increases the extraction efficiency, γ. Measured data show a qualitative agreement with theory. However, although we do not expect significant dependence on the nozzle sizes, we know from the literature that lower output is expected when the nozzle is too small, see Ref. [14]. This is in fact what we observe with a nozzle diameter of 3 mm.

We then investigate the dependency of the forward velocity on the nozzle diameter, which influences the Reynolds number characterizing the flow at the source exit. Data are shown in Fig. 7. We fit a Maxwell-Boltzmann curve to the recorded phosphorescence signal and extract a peak forward velocity. Although we observe an overall velocity reduction upon nozzle diameter enlargement, we also see large difference depending on cell length. With longer cells, CO molecules undergo more collisions and are thus more likely to diffuse to the walls. Therefore, we believe that faster molecules that spend a shorter time in the cell have a larger chance of leaving

Optics EXPRESS

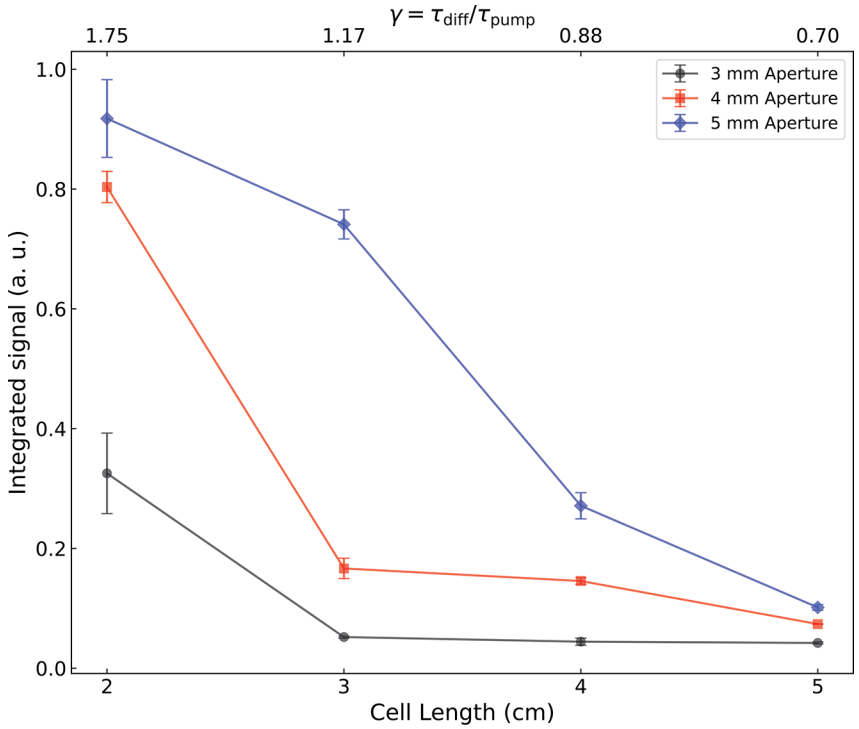

Fig. 6. Phosphorescence signal in dependence on cell length for various nozzle diameters.

the cell through the nozzle. Those faster molecules thus push the observed velocity distribution in the beam toward a larger average speed for 4 and 5-cm cell length.

With 5-mm aperture and 2-cm length of the cell, the peak of the measured signal is about 2.5×10^{14} molecules/(s sr). We form a beam that can be used as a precursor for laser cooling, as duscussed above, of about 3×10^{12} molecules/s. This can be compared with the incoming CO flow of 1 SCCM, or 4.5×10^{17} molecules/s, yielding an overall efficiency of the buffer gas cooling of about 10^{-5}, from the bottle to the beam.

Finally, we compare signal from $N = 0$ and $N = 1$ for various He flow rates. Integrated phosphorescence signal from the $a^3\Pi$ state is plotted in dependence on He flow in Fig. 8. The observed signal ratio of $N = 0$ to $N = 1$ is roughly 9:1. This is somehow surprising. In $N = 1$ there are 3 times as many states as in $N = 0$; but selection rules should not allow excitation of $M = 0$ in $N = 1$. Therefore, considering the energy difference of CO in the ground state between the two rotational states and a temperature of 4 K, we expect the ratio of $N = 0$ to $N = 1$ to be about 2:1. It is known that rotational thermalisation inside the cell with the buffer gas can be modeled in a satisfactory way. [22] So, in order to account for the observed 9:1 ratio, we should assume a temperature inside the cell below 2 K, against a measured temperature at the cell surface of 3.7 K. According to the cryostat producer, Cryomech, the 2.7 W of cooling capacity of the cryostat at 4.2 K should be sufficient to liquefy the helium that passes through the cooling coil mounted on the cryostat head. Thus, He evaporating inside the cell would lower the temperature, but the system could be far away from equilibrium and not easy to measure directly. Therefore, at present, we cannot give a definite explanation of the ratio of the two rotational states.

Optics EXPRESS

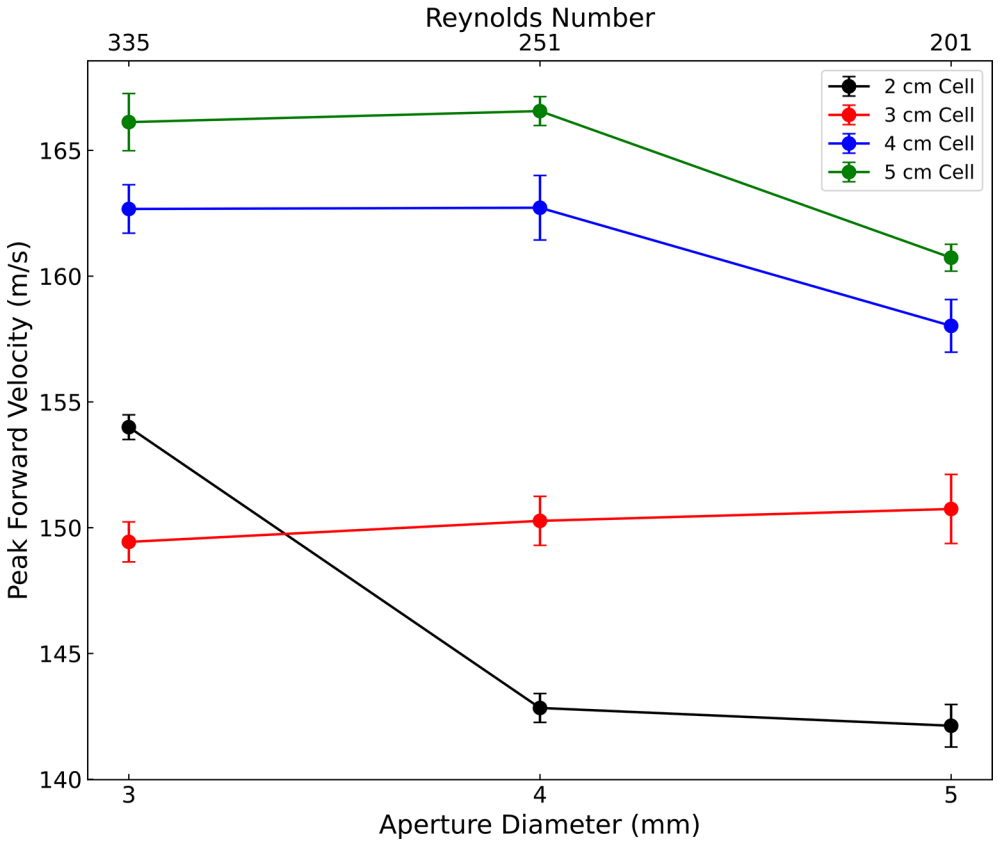

Fig. 7. Peak forward velocity in dependence on nozzle diameter for various cell lengths.

5. Conclusion

In this work, we have developed and characterized a cryogenic buffer gas cell source for the formation of continuous molecular beams. Our combined theoretical description and experimental observations contribute to the growing understanding of molecular beam formation using a buffer gas cell. By systematically varying the buffer gas flow, the length of the cooling region, and the diameter of the nozzle, our research demonstrates the impact of these parameters on key properties of the molecular beam; specifically, on cooling efficiency, molecular beam extraction, and forward velocity.

A key finding of this study is that CO molecules experience significant translational cooling, with their temperature reduced from 78 K to 7 K at optimal helium flow rates. The forward velocity of the CO molecules is influenced by the Reynolds number, while a shorter cell length enhances molecular extraction by minimizing losses due to diffusion to the walls. Additionally, a nozzle size above 3 mm provides efficient beam flux.

The source studied here can be adapted for a wide range of molecular species, providing a foundational understanding of buffer gas cell operation. These findings have important implications for the production of efficient cold molecular beam sources and their subsequent applications in precision measurements and cold molecular experiments.

Optics EXPRESS

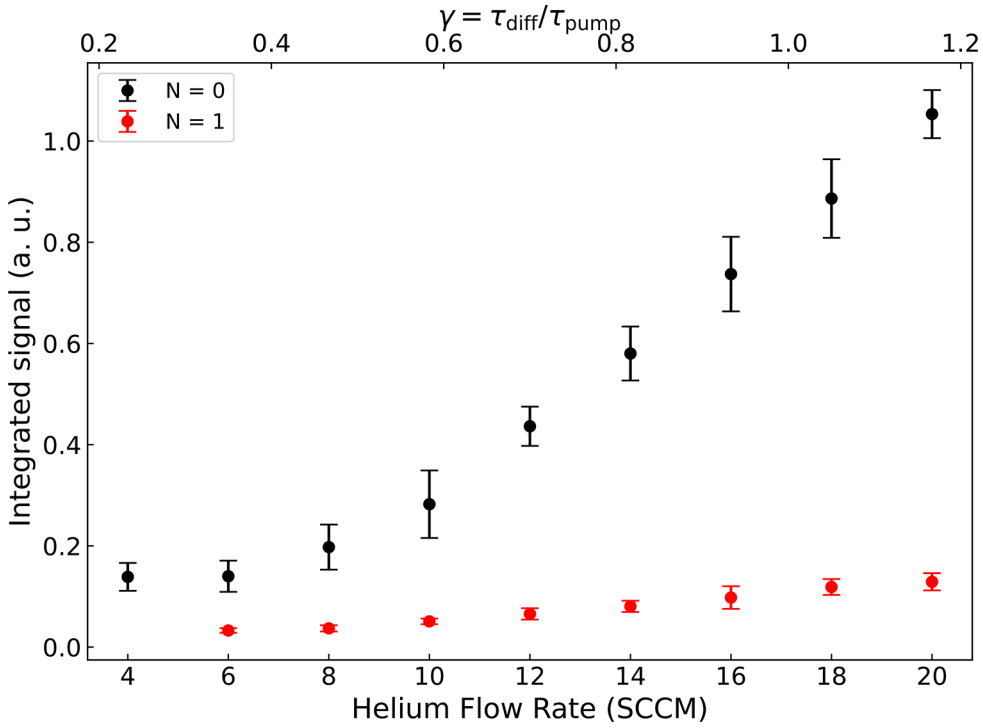

Fig. 8. Phosphorescence signal for N=0 and N=1, Cell length 3 cm and 5 mm aperture.

Funding. European Partnership on Metrology (COMOMET, FunderID: 10.13039/100019599, 23FUN04); NextGenerationEU (IR0000016, D2B8D520, B53C22001750006, ID D2B8D520, CUP B53C22001750006).

Disclosures. The authors declare no conflicts of interest

Data availability. Data underlying the results presented in this paper are not publicly available at this time but may be obtained from the authors upon reasonable request.

References

1. L. D. Carr, D. DeMille, R. V. Krems, *et al.*, "Cold and ultracold molecules: science, technology and applications," New J. Phys. **11**(5), 055049 (2009).
2. S. L. Cornish, M. R. Tarbutt, and K. R. Hazzard, "Quantum computation and quantum simulation with ultracold molecules," Nat. Phys. **20**(5), 730–740 (2024).
3. S. E. Maxwell, N. Brahms, R. deCarvalho, *et al.*, "High-flux beam source for cold, slow atoms or molecules," Phys. Rev. Lett. **95**(17), 173201 (2005).
4. N. R. Hutzler, H.-I. Lu, and J. M. Doyle, "The buffer gas beam: An intense, cold, and slow source for atoms and molecules," Chem. Rev. **112**(9), 4803–4827 (2012).
5. V. Singh, K. S. Hardman, N. Tariq, *et al.*, "Chemical reactions of atomic lithium and molecular calcium monohydride at 1 k," Phys. Rev. Lett. **108**(20), 203201 (2012).
6. Z. Lasner, D. Mitra, M. Hiradfar, *et al.*, "Fast and high-yield loading of a D_2 magneto-optical trap of potassium from a cryogenic buffer-gas beam," Phys. Rev. A **104**(6), 063305 (2021).
7. S. C. Wright, M. Doppelbauer, S. Hofsäss, *et al.*, "Cryogenic buffer gas beams of AlF, CaF, MgF, YbF, Al, Ca, Yb and NO – a comparison," Mol. Phys. **121**(17-18), e2146541 (2023).
8. N. E. Bulleid, S. M. Skoff, R. J. Hendricks, *et al.*, "Characterization of a cryogenic beam source for atoms and molecules," Phys. Chem. Chem. Phys. **15**(29), 12299–12307 (2013).
9. J. F. Barry, E. S. Shuman, and D. DeMille, "A bright, slow cryogenic molecular beam source for free radicals," Phys. Chem. Chem. Phys. **13**(42), 18936–18947 (2011).
10. S. Truppe, M. Hambach, S. M. Skoff, *et al.*, "A buffer gas beam source for short, intense and slow molecular pulses," J. Mod. Opt. **65**(5-6), 648–656 (2018).
11. A. D. White, S. Popa, J. Mellado-Munoz, *et al.*, "Slow molecular beams from a cryogenic buffer gas source," Phys. Rev. Res. **6**(4), 043232 (2024).

Optics EXPRESS

12. D. Patterson, M. Schnell, and J. M. Doyle, "Enantiomer-specific detection of chiral molecules via microwave spectroscopy," Nature **497**(7450), 475–477 (2013).
13. D. E. Oates and J. G. King, "Measurement of helium-helium scattering cross section at low temperatures," Phys. Rev. Lett. **26**(13), 735–737 (1971).
14. N. R. Hutzler, M. F. Parsons, Y. V. Gurevich, *et al.*, "A cryogenic beam of refractory, chemically reactive molecules with expansion cooling," Phys. Chem. Chem. Phys. **13**(42), 18976–18985 (2011).
15. W. C. Campbell and J. M. Doyle, "Cold molecules: Theory, experiment, applications," in *Cold Molecules: Theory, Experiment, Applications*, R. V. Krems, W. C. Stwalley, and B. Friedrich, eds. (CRC Press, 2009), Chap. 13, pp. 473–508.
16. C. D. Ball and F. C. De Lucia, "Direct measurement of rotationally inelastic cross sections at astrophysical and quantum collisional temperatures," Phys. Rev. Lett. **81**(2), 305–308 (1998).
17. N. Hutzler, "Charcoal as a helium cryopump: Version 1.0,".
18. V. Singh, A. K. Samanta, N. Roth, *et al.*, "Optimized cell geometry for buffer-gas-cooled molecular-beam sources," Phys. Rev. A **97**(3), 032704 (2018).
19. J. J. Gilijamse, S. Hoekstra, S. A. Meek, *et al.*, "The radiative lifetime of metastable CO (a^3Pi, $v = 0$)," J. Chem. Phys. **127**(22), 221102 (2007).
20. R. T. Jongma, T. Rasing, and G. Meijer, "Two-dimensional imaging of metastable co molecules," The J. Chem. Phys. **102**(5), 1925–1933 (1995).
21. L. Velarde, D. P. Engelhart, D. Matsiev, *et al.*, "Generation of tunable narrow bandwidth nanosecond pulses in the deep ultraviolet for efficient optical pumping and high resolution spectroscopy," Rev. Sci. Instrum. **81**(6), 063106 (2010).
22. S. M. Skoff, R. J. Hendricks, C. D. J. Sinclair, *et al.*, "Diffusion, thermalization, and optical pumping of YbF molecules in a cold buffer-gas cell," Phys. Rev. A **83**(2), 023418 (2011).

130.217.72.134 2025-07-23 11:58:2